Topological photonic orbital-angular-momentum switch

Xi-Wang Luo,[1,2] Chuanwei Zhang,[2,*] Guang-Can Guo,[1,3] and Zheng-Wei Zhou[1,3,†]

[1]*Key Laboratory of Quantum Information, University of Science and Technology of China, Hefei, Anhui 230026, China*

[2]*Department of Physics, The University of Texas at Dallas, Richardson, Texas 75080-3021, USA*

[3]*Synergetic Innovation Center of Quantum Information and Quantum Physics, University of Science and Technology of China, Hefei, Anhui 230026, China*

(Received 18 July 2017; published 17 April 2018)

The large number of available orbital-angular-momentum (OAM) states of photons provides a unique resource for many important applications in quantum information and optical communications. However, conventional OAM switching devices usually rely on precise parameter control and are limited by slow switching rate and low efficiency. Here we propose a robust, fast, and efficient photonic OAM switch device based on a topological process, where photons are adiabatically pumped to a target OAM state on demand. Such topological OAM pumping can be realized through manipulating photons in a few degenerate main cavities and involves only a limited number of optical elements. A large change of OAM at $\sim 10^q$ can be realized with only q degenerate main cavities and at most $5q$ pumping cycles. The topological photonic OAM switch may become a powerful device for broad applications in many different fields and motivate a topological design of conventional optical devices.

DOI: 10.1103/PhysRevA.97.043841

I. INTRODUCTION

Discrete degrees of freedom, such as charge, spin, valleys, etc., play a crucial role in many information encoding and device applications [1–4]. In this context, a fundamental degree of freedom of photons, the orbital angular momentum (OAM), possesses a unique property that an infinite number of distinctive OAM states are available [5–7]. This unique property makes photonic OAM very attractive for various applications in optical communication [8–10], quantum simulation [11–14], quantum information [15–18], and quantum cryptography (e.g., key distribution) [19–22]. To fully utilize these applications, a tunable device that can rapidly and robustly switch between different OAM modes on demand is therefore highly desirable. However, many conventional OAM switching devices rely on precise parameter control and are usually limited by slow switching rates (approximately kilohertz) [23,24] or low purity and efficiency [25,26], and limited number of usable OAM modes [27,28].

The photonic OAM is a discrete degree of freedom that characterizes the topological charge (i.e., the winding of the azimuthal phase) of a photon field with cylindrical symmetry. Therefore a natural question is whether a topological process can be designed to create a robust photonic OAM switching device with high performance. Recently, the study of topological photonics has become one frontier direction in optical physics with the major focus on modulating photon propagation through topological edge states [29–35], while practical topological photonic devices for on-demand switching of photon internal degrees of freedom are still largely lacking.

In this paper, we propose a practical photonic OAM switching device through the topological adiabatic pumping of OAM states, which is robust (immune to small perturbations in system parameters), fast (approximately megahertz switching rate), efficient ($\sim$90% efficiency and $\sim$100% purity in principle), and highly tunable (on demand switch for high-OAM states). Topological pumping was initially proposed by Thouless [36] for a periodically time-varying system, and has been recently realized in ultracold atom optical lattices [37,38] and coupled optical waveguides [39,40], where particles are adiabatically pumped in real-space lattices. Such "Thouless pumps" along particle's internal degrees of freedom have not been well explored, although atomic hyperfine states have been utilized as a synthetic dimension for studying quantum Hall effects [41–43].

Here we show how to realize Thouless pumps in the synthetic OAM space of photons where large numbers of OAM modes are available, which provides the basis for engineering a topological photonic OAM switch. Essentially, we propose a scheme to realize a tunable double-well OAM lattice (two lattice sites in each unit cell) by manipulating photons in a single degenerate main cavity, where photons can be adiabatically pumped to target OAM lattice sites (i.e., the OAM states). Thanks to the topological nature of the pumping, a precise switch can be realized without involving precise control of the parameters during the pumping cycle. Such robustness of the pumping against perturbations as well as its properties in the presence of photon losses are considered. Moreover, even though the pumping process is adiabatic, the pumping cycle can be very short. With realistic optical elements, it is possible to achieve a switching rate of approximately megahertz, which is much faster than commonly used OAM switching devices [23,24]. Even for a large change of OAM at $\sim 10^q$, only q degenerate main cavities and at most $5q$ pumping cycles are needed using a multistage setup, leading

*chuanwei.zhang@utdallas.edu
†zwzhou@ustc.edu.cn

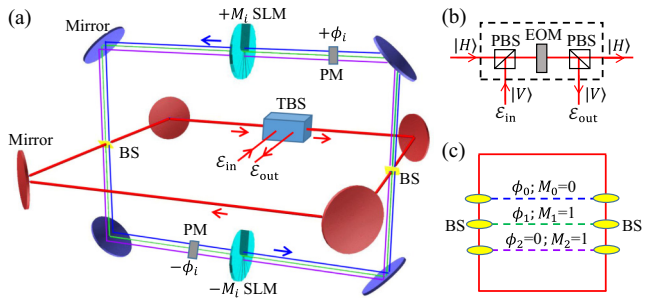

FIG. 1. (a) Experimental photonic circuit for a degenerate cavity system. The main cavity (red curved mirrors) is coupled with auxiliary cavities (blue curved mirrors) by beam splitters (BSs). A tunable beam splitter (TBS) is used to tune the coupling between the cavity (in H polarization) and the input/output fields (in V polarization). (b) Optical design for the TBS. (c) Schematic diagram of the system with three auxiliary cavities (dashed lines), with corresponding tunneling phase ϕ_s and step M_s as labeled.

to exponential speedup of the OAM switch. The proposed topological photonic OAM switch only relies on a simple optical setup with a few degenerate main cavities, therefore it may become a powerful device for broad applications in quantum information and optical communications. Our proposed topological approach for device engineering may go beyond the OAM switch and inspire the topological design of conventional optical devices.

II. THE SYSTEM

As shown in Fig. 1(a), our system contains a main degenerate multimode cavity [44–48], which supports a large number of OAM modes and is coupled with three degenerate auxiliary cavities by beam splitters (BSs). The degenerate cavities used in our scheme possess fully transverse degeneracy and their design principle is based on the round-trip Gauss matrix [often called the $ABCD$ ray matrix with A,D (B,C) diagonal (off-diagonal) matrix elements] [44]. We consider a ring-type cavity possessing cylindrical symmetry with respect to the optical axis; the cavity modes are Laguerre-Gaussian (LG) modes $E_{p,l}$ with radial index p and azimuthal index l. The resonance frequencies of the LG modes are [49,50]

$$\omega_{p,l} = n\Omega_{\rm F} + (2p + |l| + 1)\frac{\arccos\left(\frac{A+D}{2}\right)}{2\pi}\Omega_{\rm F}, \qquad (1)$$

where the integer n is the longitudinal mode index that is fixed in our scheme and $\Omega_{\rm F}$ is the free spectral range (FSR) of the cavity. The off-diagonal ray matrix elements B and C only affect beam waist size. The degenerate cavity is obtained when the round-trip $ABCD$ ray matrix is equal to identity [44], which can be achieved using curved mirrors or intracavity lenses. In this case, all transverse LG modes $E_{p,l}$ have the same resonance frequency $n\Omega_{\rm F}$, yielding a degenerate cavity supporting different OAM modes l for photons. The tunneling between different OAM states is realized by spatial light modulators (SLMs). The unimportant radial index p, which is related to the radial mode profile of the input photons, is omitted. There are many ways to construct a degenerate cavity; for example, we consider a rectangular-shaped cavity shown in Fig. 1(a) formed by four identical curved mirrors with focal length equal to optical path length between adjacent mirrors (see Appendix A). We use a tunable beam splitter (TBS) to couple the cavity with the outside world; it is realized by sandwiching an electro-optic modulator (EOM) [49] between two polarizing beam splitters (PBSs), as shown in Fig. 1(b). The EOM rotates the photon's polarizations in a tunable way as $|H\rangle \to \sqrt{1-r_{\rm P}^2}|H\rangle + r_{\rm P}|V\rangle$ and $|V\rangle \to \sqrt{1-r_{\rm P}^2}|V\rangle - r_{\rm P}|H\rangle$, with $|H\rangle$ and $|V\rangle$ the horizontal and vertical polarization states which are separated by the PBS. The tunable coefficient $r_{\rm P}$ acts as the reflectivity of the TBS.

The beam splitters divert a small portion of the main-cavity photons towards the sth auxiliary cavity, and merge them back after passing through SLMs [51,52], which changes the OAM state by $\pm M_s$. This corresponds to tunnelings between different OAM states in the main cavity, with a tunneling rate determined by the reflectivities of the BSs. During the tunneling, the photon can also acquire a phase determined by the optical path-length difference between two arms of the auxiliary cavity, which can be generated and tuned using high-speed phase modulators (PMs). The system is equivalent to a one-dimensional (1D) lattice model with the lattice sites represented by the OAM states [13–15]. The Hamiltonian is given by (see Appendix A)

$$H = -\sum_{l}\sum_{s=0}^{2} J_s e^{i\phi_s} a_{l+M_s}^{\dagger} a_l + \text{H.c.}, \qquad (2)$$

where a_l is the annihilation operator of the cavity photon in the OAM state l, and M_s is the step index of the SLMs in the sth auxiliary cavity with the tunneling amplitude J_s and phase $\phi_s = l\alpha_s + \beta_s$. The PM contains a beam rotator [53] and an EOM [49]: the beam rotator, realized by two Dove prisms rotated by $\alpha_s/2$ with respect to each other, is used to generate the l-dependent phase $l\alpha_s$, and the EOM is used to tune the l-independent phase β_s.

The auxiliary cavities are designed as $\phi_2 = 0$, $M_0 = 0$, $M_1 = M_2 = 1$, and $J_1 = J_2$, as shown in Fig. 1(c). Therefore the Hamiltonian describes a generalized Aubry-André-Harper (AAH) model [54] with modulations in on-site energy, tunneling phase, and amplitude, the periods of which are determined by α_0 and α_1. Here, we focus our discussion on $\alpha_0 = \alpha_1 = 2\pi \times \frac{1}{2}$, in analogy to the Rice-Mele model (i.e., double-well superlattice model) [55] with neighboring site energy detuning $\Delta \equiv -4J_0\cos(\beta_0)$ and inter- and intra-cell tunnelings $J_\pm \equiv J_1[1 \pm e^{i\beta_1}]$ [see Fig. 2(a)]. We rewrite the Hamiltonian as

$$H = -\sum_j J_+ b_{j,2}^{\dagger} b_{j,1} + J_- b_{j+1,1}^{\dagger} b_{j,2} + \text{H.c.} + \sum_j \frac{\Delta}{2}(b_{j,1}^{\dagger} b_{j,1} - b_{j,2}^{\dagger} b_{j,2}), \qquad (3)$$

where we have introduced the unit-cell index j with $b_{j,1} = a_{2j}$ and $b_{j,2} = a_{2j+1}$. After a Fourier transformation $b_{k,1(2)} \propto \sum_j e^{ijk} b_{j,1(2)}$, the Hamiltonian in the Bloch basis becomes

$$H = -\sum_k [b_{k,1}^{\dagger}, b_{k,2}^{\dagger}] H_k [b_{k,1}, b_{k,2}]^T, \qquad (4)$$

with the Bloch Hamiltonian $H_k(t) = \mathbf{h}(k,t)\cdot\vec{\sigma}$, where $\vec{\sigma} = (\sigma_x, \sigma_y, \sigma_z)$ are the Pauli matrix and the real vector $\mathbf{h}(k,t)$ satisfies $h_x(k,t) + ih_y(k,t) = -[J_+(t) + J_-^*(t)e^{-ik}]$,

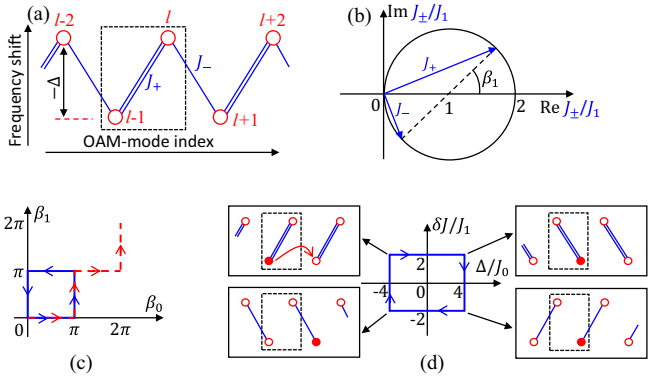

FIG. 2. (a) Diagram of the effective lattice in the OAM dimension. Each unit cell (enclosed by the dashed square) contains two sites with detuning $\Delta = -4J_0\cos[\beta_0(t)]$. $J_\pm = J_1[1 \pm e^{i\beta_1(t)}]$ are the inter- and intra-cell tunnelings, respectively, the dependence of which on the tunneling phase β_1 is shown in (b). (c) The pumping loop in the β_0-β_1 plane. Since the tunneling phase has a period of 2π, their choice is not unique, and the two loops (red dashed and blue solid) have the same topology. (d) Illustration of the pumping process. The loop in the δJ-Δ plane can be realized by either loop shown in (c). The red solid circle represents a site occupied by a photon, which moves to the right by two sites (one unit cell) during one pumping cycle.

and $h_z(k,t) = \frac{\Delta(t)}{2}$. The band structure and the Bloch wave function $e^{ikj}|u_n(k)\rangle$ can be obtained by solving $H_k|u_n(k)\rangle = E_n|u_n(k)\rangle$, with band spectrum $E_\pm = \pm|\mathbf{h}(k,t)|$. The parameters $\Delta = -4J_0\cos(\beta_0)$ and $J_\pm = J_1(1 \pm e^{i\beta_1})$ depend on the time-varying phases $\beta_{0,1}(t)$ [see Fig. 2(b)], as does the Hamiltonian $H(t)$.

III. TOPOLOGICAL PUMPING

Topological pumping was first proposed by Thouless for fermionic systems [36]. Consider a fermionic system with the same single-particle Hamiltonian as $H(t)$; if the Hamiltonian is modulated adiabatically and periodically without closing the band gap, the amount of transported particles (along the OAM space) for a filled band is characterized by the Chern number defined as the change in polarization during one pump cycle (i.e., the center-of-mass displacement of the Wannier function), which is

$$\mathcal{C}_n = \frac{1}{2\pi}\int_0^T dt \int_0^{2\pi} dk\,\Omega_{kt} \tag{5}$$

with

$$\Omega_{kt} = \langle\partial_t u_n(k,t)|\partial_k u_n(k,t)\rangle - \langle\partial_k u_n(k,t)|\partial_t u_n(k,t)\rangle.$$

The Chern number also equals to the winding number of $\pm\mathbf{h}(k,t)$ surrounding the origin as t varies over one period and k varies over the Brillouin zone. The two bands are gapped in the parameter space except the critical point when $\Delta = |J_+| - |J_-| = 0$. It can be proven that a loop which encloses the critical point is topologically nontrivial. For a clockwise loop enclosing the critical point, we find that $\mathcal{C}_\pm = \mp 1$. The Chern number is equal to the winding number of $\pm\mathbf{h}(k,t)$ surrounding the origin as t varies over one period and k varies over the Brillouin zone.

Photons are noninteracting bosons, so the photonic pumping is reduced to single-particle pumping, which is different from the fermionic pumping of a filled band. We consider a single photon in the nth band

$$|\Psi(j,0)\rangle = \sum_k \psi_k e^{ijk}|u_n(k,0)\rangle, \tag{6}$$

the modulation is adiabatic so that it will follow the initial band, and also k is a good quantum number during the pumping. So, the final state can be written as

$$|\Psi(j,t)\rangle = \sum_k \psi_k e^{ijk} e^{-i\int_0^t dt' E_n(k,t')} e^{i\gamma_n(k,t)}|u_n(k,t)\rangle, \tag{7}$$

with $\gamma_n(t)$ the Berry phase given by

$$\gamma_n(k,t) = i\int_0^t \langle u_n(k,t')|\partial_{t'}u_n(k,t')\rangle dt'. \tag{8}$$

The center of mass of the particle is

$$\begin{aligned}\bar{j}(t) &= \sum\nolimits_j \langle\Psi(j,t)|j|\Psi(j,t)\rangle \\ &= \sum_k \langle\widetilde{\Psi}(k,t)|i\partial_k|\widetilde{\Psi}(k,t)\rangle\end{aligned} \tag{9}$$

with

$$|\widetilde{\Psi}(k,t)\rangle = \psi_k e^{-i\int_0^t dt' E_n(k,t')} e^{i\gamma_n(k,t)}|u_n(k,t)\rangle. \tag{10}$$

So we have

$$\bar{j}(t) = \sum\nolimits_k i\psi_k^*\partial_k\psi_k + \int_0^t I(t')dt' \tag{11}$$

with the average current given by

$$I(t) = \sum_k |\psi_k|^2[\partial_k E(k,t) + \Omega_{kt}]. \tag{12}$$

So the displacement after one pumping cycle would be

$$\Delta\bar{j} = \bar{j}(T) - \bar{j}(0) = \int_0^T I(t)dt. \tag{13}$$

For the simple case with $\psi_k = \frac{1}{\sqrt{N}}$, N is the total number of lattice sites, $|\Psi(j,0)\rangle$ is reduced to the Wannier function $|W_n(j,0)\rangle$,

$$|\Psi(j,0)\rangle = \sum_k \frac{1}{\sqrt{N}} e^{ijk}|u_n(k,0)\rangle \equiv |W_n(j,0)\rangle, \tag{14}$$

and we have

$$\Delta\bar{j} = \frac{1}{N}\sum_k \int_0^T \Omega_{kt}dt = \int_0^T dt \int_0^{2\pi}\frac{dk}{2\pi}\Omega_{kt} = \mathcal{C}_n. \tag{15}$$

We can see that the average displacement is exactly quantized even for a single-particle Wannier state.

We consider a pumping process as shown in Fig. 2(c), where the pumping cycle corresponds to a loop in the two-dimensional parameter space spanned by β_0 and β_1. The two bands of the system are gapped in the parameter space except at the critical point $\beta_0 = \beta_1 = \pi/2$ with $\Delta = \delta J = 0$ and $\delta J \equiv |J_+| - |J_-|$. A loop which encloses this critical point is topologically nontrivial, and the topology of the pump is invariant under deformation of the loop without cutting through the critical point. Therefore it is more convenient to consider

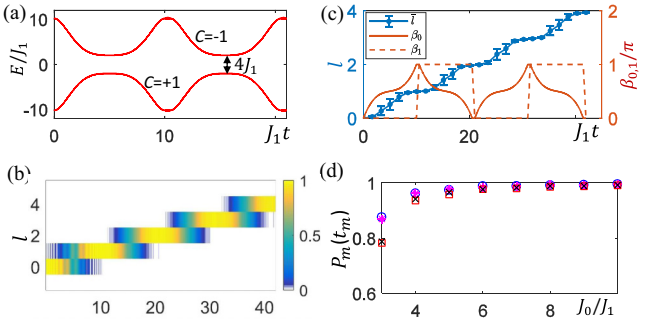

FIG. 3. (a) The band structure in one pump cycle with Chern number $\mathcal{C} = \pm 1$ for two bands. (b) Cavity photon distribution in two pump cycles with steplike transport. $P_l(t)$ is the probability of the photon in OAM state l at time t. (c) Center-of-mass displacements (dots) and their standard deviations (error bars), which are calculated by assuming Gaussian distributed random disorders $\delta\beta_{0,1}$ in the tunneling phases with standard deviations $\sigma(\delta\beta_{0,1}) = 0.1$ rad. (d) The final-state purities at $\frac{m}{2}$ pump cycles ($t_m = \frac{mT}{2}$) vs different coupling ratio J_0/J_1. The pink stars, blue cycles, black crosses, and red squares correspond to $m = 1, 2, 3$, and 4, respectively. The modulation of the pump parameters is chosen to satisfy the adiabatic condition with period $T = 21/J_1$, the temporal profiles of which are shown in (c) with β_0 the red solid line and β_1 the red dashed line. (b)–(d) The initial OAM state is $l_0 = 0$. (a)–(c) The coupling ratio is $J_0/J_1 = 5$.

the pump in the Δ-δJ plane, with corresponding pump loop and photon movement illustrated in Fig. 2(d).

The band structures ($E_\pm = \pm|\mathbf{h}(k,t)|$) along the pumping loop are shown in Fig. 3(a), with a smallest band gap $4J_1$. The two gapped bands have different transport properties due to their different topologies, characterized by Chern number $\mathcal{C} = \mp 1$, respectively. We start the pumping at $\delta J = 2J_1$ and $\Delta = -4J_0$ with $J_0 \gg J_1$, where the Wannier functions are well localized at a single OAM state (since the intercell tunneling J_- vanishes and intracell tunneling J_+ is very weak compared to detuning Δ). We consider a lower-band state with a single photon initialized at OAM state l_0 (this can be realized by resonantly feeding a single-photon pulse carrying the corresponding OAM into the cavity), which will be pumped to $l_0 + 2$ after one cycle (each unit cell contains two sites). The photon distribution and displacement of its center of mass are shown in Figs. 3(b) and 3(c). We can see a clear steplike displacement as expected. The transport is topologically protected and robust against perturbations in the parameter modulation loop. Figure 3(c) shows the center-of-mass displacement and its variation caused by the random shifts in the phase β_0 and β_1, demonstrating that the quantized transport is almost immune to such small errors.

To obtain a final state with a high purity (defined as the probability of finding the photon in the desired OAM state), a large J_0/J_1 is required to make the Wannier function well localized at a single OAM state. This is because, at the beginning (end) of the pumping, we have two flat bands with $E_\pm = \pm\sqrt{4J_0^2 + 4J_1^2}$, and the eigenvectors $|u_-(k,0)\rangle = [\cos(\theta), -\sin(\theta)]$ $|u_+(k,0)\rangle = [\sin(\theta), \cos(\theta)]$, with $\tan(2\theta) = J_1/J_0$ independent of k. The Wannier function of the lower band is $|W_-(0)\rangle = \cos(\theta)|l = 0\rangle - \sin(\theta)|l = 1\rangle$, which is well localized on $l = 0$ for $J_1/J_0 \ll 1$. As a result, the pumping of state $|l = 0\rangle$ is characterized by the lower band which gives a quantized transport of $\mathcal{C}_- = 1$. In addition, different from the pumping of a whole filled band, the final state is not a simple displacement of the initial state for single-particle pumping; this is because there exists diffusion during the pumping due to the dynamical phase $e^{-i\int_0^T dt E_n(k,t)}$, which decreases the purity of the final state. The diffusion leads to a wider profile of its density distribution, and induces minor populations of unwanted OAM states. To reduce such effect, we need to make the band as flat (in momentum space) as possible during the pump, then the dynamical phase becomes a constant phase independent of k. During the pump, the bands are given by

$$E_\pm = \pm\sqrt{4J_0^2 + |J_+^* + J_- e^{ik}|^2}$$
$$\simeq \pm\left\{2J_0 + \frac{J_1^2}{J_0} + \frac{J_1^2}{4J_0}[\cos(k) - \cos(k + 2\beta_1)]\right\}, \quad (16)$$

which is always flat for $\beta_1 = 0,\pi$. As we modulate β_1 from zero (π) to π (zero), such that J_+ (J_-) changes from $2J_1$ to zero while J_- (J_+) changes from zero to $2J_1$, the bands are approximately flat in the limit $J_1/J_0 \ll 1$, and the diffusion effect is negligible. The band gap is also very large during this modulation, and the diffusion effect can be reduced further by increasing the modulating speed properly. These effects are verified by our numerical calculation of the purity for different values of J_0/J_1 [see Fig. 3(d)]. The purity can be close to 100% by using a larger value of J_0/J_1.

Each pumping cycle shifts the photon's OAM by 2, therefore even switching numbers can be realized by integer pumping cycles. However, we notice that the photon's OAM state is also well localized at half-integer pumping cycles with OAM shifted by an odd number [see Figs. 3(b)–3(d)], therefore odd switching numbers can be realized by half-integer pumping cycles. Alternatively, we can design the synthetic double-well lattice such that two sites in each unit cell are represented by different polarization states with the same OAM, and each pumping cycle changes the photon's OAM by 1. Similarly, we can put the photon in the upper band, then the above pumping will change its OAM by -1 or -2; alternatively, this can also be achieved by considering a counterclockwise pumping loop and a photon in the lower band. The system is linear (with no photon-photon interaction); as a result, our scheme can simultaneously switch multiple photons in different OAM modes, each pumping cycle shifting the OAM by $+2$ (-2) for photons in the lower (upper) band.

IV. TOPOLOGICAL OAM SWITCH

Such quantized transport offers a robust way to switch the OAM states of photonic signals in three steps: (i) input—the input photon pulse enters the cavity and the l_0 cavity mode is excited; (ii) topological pumping—the photon is pumped to the desired OAM state; and (iii) output—the photon pulse is released out of the cavity. The input and output are realized by a TBS which couples the cavity with the outside world. The tunability of the input/output beam splitter is crucial for improving the efficiency of the OAM switch because the coupling between the cavity and the outside world needs to be

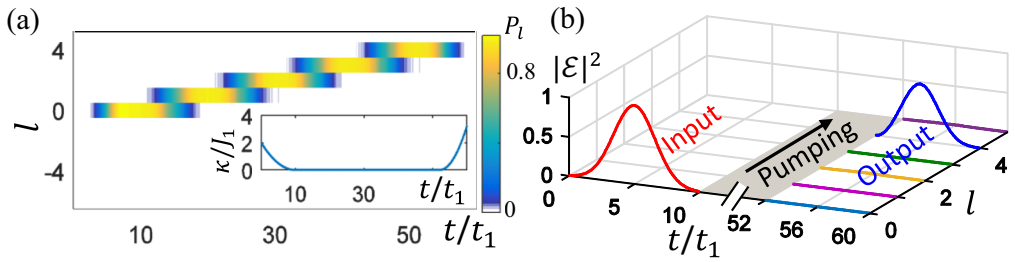

FIG. 4. (a) Normalized cavity photon distribution and (b) input/output photon pulses during the OAM switching. The normalized input pulse is $\mathcal{E}_{\rm in}(t) = e^{-iE_-t-0.2(J_1t-5)^2}$ with $l_0 = 0$ (i.e., only the zero-OAM Wannier orbital is excited). E_- is the lower band energy. After the input pulse enters the cavity, we pump the state to higher OAM modes, and then release the signal by increasing the cavity loss κ [see the inset in (a)]. Other parameters are the same as in Fig. 3(b).

turned on during input/output so that the signals can get in/out, and turned off during the pumping to avoid unwanted photon losses. The dynamics are characterized by [56]

$$\dot{a}_l = \frac{1}{i}[a_l, H] - \frac{\kappa}{2}a_l + \delta_{l,l_0}\sqrt{\kappa_{\rm e}}\mathcal{E}_{\rm in}(t),$$

where $\mathcal{E}_{\rm in}(t)$ is the input photonic field in the l_0 OAM state, κ is the total photon loss, and the tunable coupling strength between the cavity and the input/output fields is $\sqrt{\kappa_{\rm e}} \simeq |r_{\rm P}|\sqrt{\frac{\Omega_{\rm F}}{2\pi}}$ [57] with $r_{\rm P}^2 \ll 1$ and $\Omega_{\rm F}$ the FSR of the main cavity.

In an ideal case, all optical elements are perfectly designed, and the only photon loss channel is the TBS, so we have $\kappa = \kappa_{\rm e}$. With proper modulation of $\kappa_{\rm e}$ (i.e., $r_{\rm P}$), the input signal pulse can enter the cavity with an efficiency as high as 90%. Then it is pumped to the desired OAM state and finally released from the cavity. The evolution of the photon field inside the cavity, as well as the temporal profiles of input/output fields and photon loss κ, are shown in Figs. 4(a) and 4(b). We see that photons are almost perfectly transported to the desired OAM state, but the intensity is slightly reduced due to photon losses during input and diffusion during pumping.

V. EXPERIMENTAL CONSIDERATION

Typically the FSR of the main cavity is $\Omega_{\rm F} \sim 2\pi \times 1$ GHz, and the tunneling strength, given by $J_s = \Omega_{\rm F}\frac{|r_s|^2}{2\pi(1+|t_s|^2)}$ with r_s (t_s) the reflectivity (transmissivity) of the corresponding beam splitters [13–15,30], can be up to tens of megahertz (e.g., $J_0 \sim 2\pi \times 20$ MHz and $J_0 \gg J_1 \sim 2\pi \times 4$ MHz). The pump period $T \sim 20/J_1$ leads to a switching time of the order of microseconds. Notice that the bandwidth of the input signal pulse should be smaller than the initial band gap $4J_0$, leading to a bandwidth of the order of 10 MHz for the input photon, and such photon source can be realized using cavity-enhanced parametric downconversion [58]. The upper limit ($l_{\rm max}$) that the OAM state can be switched to is determined by the aperture of the optical elements because the beam size increases with the OAM number l. For typical mirror size, $l_{\rm max}$ can be very large (hundreds), leading to a switchable OAM range $l \in [-l_{\rm max}, l_{\rm max}]$. Imperfections such as extra photon losses may be introduced by cavity mirrors, TBS, phase modulators, and SLMs. Such losses only reduce the intensity of the output field without affecting the quantized switching (see Appendix B). To reduce such extra losses, we can make use of high-efficiency intracavity elements (e.g., EOM, SLM, etc.) with high transmission (through antireflection coating); it is possible to make these extra losses as small as a few tens of kilohertz (much smaller than the switching rate of megahertz) [51,59–61]. Also, the defects in the SLMs would induce an imperfect switch; fortunately, only two high-efficiency SLMs (which can be fabricated with high precision [51]) are used and photons may pass the SLMs many times to realize high switch distance. Deviations from cavity degeneracy lead to random on-site energy shifts $\delta\omega_l \sim |l|\delta\omega$ (see Appendix C). Due to the topological protection, our scheme works well as long as the shift for the maximal OAM state (hundreds) is smaller than the smallest band gap $l_{\rm max}\delta\omega \lesssim 4J_1$ (see Appendix C). This requires that the accuracy of the mirror (lens) distance should be of the order of micrometers, which can be realized using a high-precision translation stage. Thanks to the degenerate-cavity setup with all OAM modes sharing the same optical paths, disorders in the tunneling coefficients are negligible since all tunnelings are realized by the same sets of auxiliary cavities and can be controlled simultaneously. Other imperfections, such as a global shift in the resonance frequency of the degenerate cavity, will not affect the pumping. Therefore, our scheme should be feasible even in the presence of realistic imperfections.

VI. MULTISTAGE GENERALIZATION

To obtain high OAM states, large numbers of pump cycles may be required, which slow down the switching rate. To

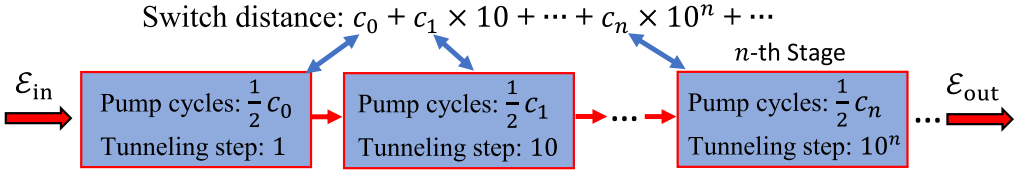

FIG. 5. Illustration of a multistage setup with $N = 10$. Each half pump cycle shifts the OAM by the corresponding tunneling step.

accelerate the switching rate, we consider a multistage setup with several cascaded degenerate-cavity systems as shown in Fig. 5. In the nth stage, we choose the tunneling step of the SLMs as $M_1 = M_2 = N^n$ with N an integer, and $\alpha_0 = \alpha_1$ satisfying $\mathrm{mod}(\alpha_0 N^n, 2\pi) = \pi$. For an arbitrary switching distance $\Delta l = \sum_n c_n N^n$ (with c_n the expansion coefficients), the corresponding pump cycle of the nth stage is $c_n/2$, which gives the total switching time $T \sum_n c_n/2$. For example, considering $\Delta l = 512$ and $N = 10$, the total switching time is only $4T$. Both the maximum number of stages $\leqslant \log_N l_{\max}$ and the maximum switching time $\leqslant \frac{TN}{2} \log_N l_{\max}$ are logarithmic, yielding exponential speedup for the OAM switch.

VII. DISCUSSION AND CONCLUSION

A conventional spatial light modulator [23] and digital micromirror device [24] are limited by the switching rates of approximately kilohertz. Higher switching rates can be achieved by combining an acousto-optic (electro-optic) modulator with SLMs (q plate) [25,28], or using on-chip resonators [26]. However, the acousto-optic modulator would induce unwanted change in wavelength, and the on-chip switching has a very low efficiency. Moreover, all these approaches require precise control of experimental parameters and the number of usable OAM modes is usually very limited. In contrast, our scheme is robust against perturbations due to its topological feature, and is also able to rapidly switch to high OAM modes with high efficiency. Our results of single-photon pumping can be generalized to multiphoton states or even classic coherent states. Since the system is linear with no interaction, every photon is pumped independently.

In summary, we proposed a topological photonic OAM switch which is fast, robust, efficient, and accessible to exponentially large OAM states. The proposed topological pumping in the OAM-based synthetic dimension offers a powerful platform to study 1D topological physics of the generalized AAH model. The simple optical setup for the topological photonic OAM switch opens a wide range of experimental opportunities and may find important applications in quantum information processing and optical communications.

ACKNOWLEDGMENTS

This paper is funded by National Natural Science Foundation of China (Grants No. 11574294 and No. 61490711), National Key Research and Development Plan (Grants No. 2016YFA0301700 and No. 2016YFA0302700), the "Strategic Priority Research Program(B)" of the Chinese Academy of Sciences (Grant No. XDB01030200), U.S. Army Research Laboratory's Army Research Office (Grant No. W911NF-17-1-0128), AFOSR (Grant No. FA9550-16-1-0387), and NSF (Grant No. PHY-1505496).

APPENDIX A: THE CAVITY STABILITY AND EFFECTIVE HAMILTONIAN

There are many ways to construct a degenerate cavity, and its stability may depend on specific configuration. For example, we consider a rectangular-shaped cavity shown in Fig. 1(a) in the main text with width X and length Y. Four curved mirrors are identical with the focal length F and the fully

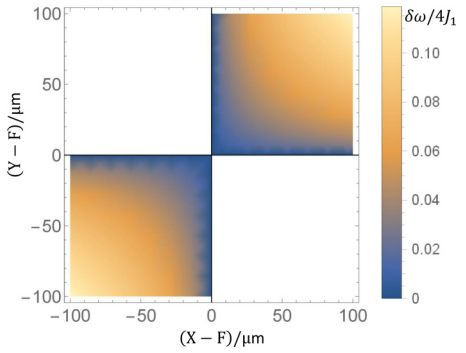

FIG. 6. Plot of frequency difference $\delta\omega$ between adjacent OAM modes normalized to the band gap $4J_1$ with respect to the width and length of the rectangular cavity. The white regions represent configurations where the cavity is unstable. Our scheme works well if $|l|\frac{\delta_\omega}{4J_1} \lesssim 1$. Other parameters are $F = 10$ cm, $J_1 = 0.004\Omega_F$.

transverse degeneracy can be obtained for $X = Y = F$. The cavity is stable for $(X - F)(Y - F) >= 0$ and unstable for $(X - F)(Y - F) < 0$ (see Fig. 6). In the stable region, the beam waist is given by $w_0^2 = \frac{\lambda F}{2\pi}\sqrt{\frac{X-F}{Y-F}}$ with λ the wavelength, and w_0 is of the order of 1 mm. These properties are similar to those for the confocal Fabry-Perot cavity [49,50]. Because the cavity possesses cylindrical symmetry with respect to the optical axis, ellipsoidal (rather than spherical) mirrors are used to correct astigmatism caused by non-normal reflections. Alternatively, this can be done by replacing the curved mirror with an intracavity lens and a plane mirror, or by changing the geometry of the cavity.

Inserting BSs may slightly adjust the optical path length of the cavity and thereby the $ABCD$ ray matrix, which can be restored easily to identity by modifying X or Y. The beam splitters divert a small portion of photons in the main cavity to the auxiliary cavity containing two SLMs, which induce tunnelings between different OAM modes. To show this, we first consider a single auxiliary cavity with two ± 1 SLMs. Our system is equivalent to a 1D lattice of a coupled cavity array with lattice sites represented by different OAM modes [13–15], as shown in Fig. 7. The optical path length of the auxiliary cavity is chosen for destructive interference so that photons spend most of the time in the main cavity (small imperfections of the auxiliary cavity can be ignored because of this). The system is characterized by the following

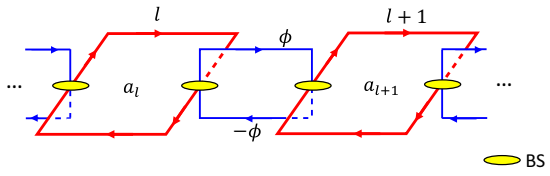

FIG. 7. The equivalent circuit in the OAM space, with ϕ the phase imbalance between two arms of the auxiliary cavity and a_l the field operator for OAM mode l. The red (blue) loop represents the main (auxiliary) cavity.

tight-binding Hamiltonian [30]:

$$H = -\sum_l J e^{i\phi} a_{l+1}^\dagger a_l + \text{H.c.}, \tag{A1}$$

where a_l is the annihilation operator of the cavity photon in the OAM state l; J and ϕ are corresponding tunneling amplitude and phase, which are determined by reflectivities of the BSs and the optical path length of two arms of the auxiliary cavity, respectively. It is straightforward to generalize the results to multiauxiliary cavities. Using three properly designed auxiliary cavities, we obtain the Hamiltonian Eq. (1) in the main text. Without tunnelings, the system has a single trivial flat band since all OAM modes are degenerate. The tunneling and interference between different OAM modes lead to nontrivial topological band structures, based on which we can switch OAM states through topological pumping.

APPENDIX B: EFFECTS OF PHOTON LOSSES

Typically, the optical path length of the cavity is about tens of centimeters, which leads to a FSR $\Omega_F = 2\pi c/L \sim 2\pi \times 1$ GHz, where L is the optical path length of the cavity and c is the speed of light. The reflectivity r_P of the TBS can be tuned by the EOM. If the tuning rate is much smaller than the FSR Ω_F, its effect is well characterized by a time-dependent coupling $\sqrt{\kappa_e(t)} \simeq |r_P(t)|\sqrt{\frac{\Omega_F}{2\pi}}$, where κ_e can be tuned from zero to a few megahertz within a few microseconds and vice versa. In realistic experiments, there are other photon losses due to factors such as the finite Q factor of the cavity, the intrinsic loss of the SLMs, and phase modulators. Such photon loss can be made as low as tens of kilohertz (much smaller than the switching rate) using high-performance optical elements. For extremely high OAM states, the beam size becomes comparable with the aperture of the optical elements, which gives an upper limit that the OAM can be switched to. We consider the pumping between OAM states smaller than the upper limit; the dynamics of the lossy system is characterized by the master equation

$$\dot{\rho} = \frac{1}{i}[H,\rho] + \kappa_0 \sum_l \left(a_l \rho a_l^\dagger - \frac{1}{2}\rho a_l^\dagger a_l - \frac{1}{2} a_l^\dagger a_l \rho \right) \tag{B1}$$

with photon loss rate κ_0. For the pumping of a single-photon state, the solution is simply given by

$$\rho = (1 - e^{-\kappa_0 t})|\text{vac}\rangle\langle\text{vac}| + e^{-\kappa_0 t}|\Psi(t)\rangle\langle\Psi(t)|, \tag{B2}$$

with $|\Psi(t)\rangle$ the solution of the nondissipative case. The photon density distribution

$$N(l,t) = \frac{\text{Tr}[\rho(t) a_l^\dagger a_l]}{\sum_l \text{Tr}[\rho(t) a_l^\dagger a_l]} = \langle\Psi(t)|a_l^\dagger a_l|\Psi(t)\rangle \tag{B3}$$

is the same as the nondissipative case, except that the probability to find the photon inside the cavity is reduced to $e^{-\kappa_0 t_p}$ with t_p the total pumping time. Our system is linear with no interactions, thus the results of single-photon pumping can also be generalized to multiphoton states and even classic coherent states.

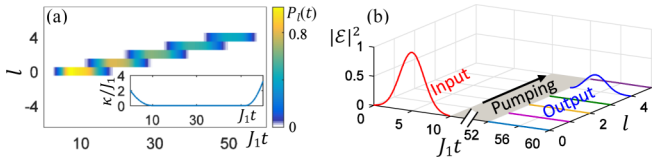

FIG. 8. (a) Normalized cavity photon distribution and (b) input/output photon pulses in the OAM switching. The parameters are the same as in Fig. 4 in the main text, except that the photon loss is nonzero during the pumping with $\kappa_0 = 0.02J_1$.

When the cavity is coupled with the input/output signals, the dynamics are characterized by the Langevin equation

$$\dot{a}_l = \frac{1}{i}[a_l, H] - \frac{\kappa}{2} a_l + \delta_{l,l_0}\sqrt{\kappa_e}\mathcal{E}_{\text{in}}(t), \tag{B4}$$

with $\kappa = \kappa_0 + \kappa_e$ and $\mathcal{E}_{\text{in}}(t)$ the input optical field in the l_0 OAM state which can be either a single-photon pulse or a classic coherent pulse. The dynamics of both the single-photon and coherent input signal are described by Eq. (B4), with a_l being the coherent (single-photon) amplitude of OAM state l. Typically, the intrinsic photon loss κ_0 is of the order of tens of kilohertz (which can be made even smaller by improving the performance of the optical elements), and it only reduces the switching efficiency without affecting the quantized transport (even for a strong loss), as shown in Fig. 8 with a large κ_0 ($\sim 2\pi \times 100$ kHz).

APPENDIX C: EFFECTS OF DEVIATIONS FROM THE DEGENERACY POINT

In the ideal case, the cavities always stay at the degeneracy point when the $ABCD$ matrix is equal to identity. Deviations from the degeneracy point lead to a frequency shift $(2p + |l| + 1)\Omega_F \arccos(\frac{A+D}{2})$ to the LG cavity modes. This would hardly affect tunnelings because the BS reflectivity is not affected and the optical path length of the auxiliary cavity is chosen for destructive interference (photons spend most of their time in the main cavity). For the OAM states considered in our system, the radial index p is of the same order of magnitude as $|l|$ (though each OAM mode may contain multiple p components). Overall, deviations from degeneracy lead to a random energy shift $\delta\omega_l a_l^\dagger a_l$ to each OAM mode,

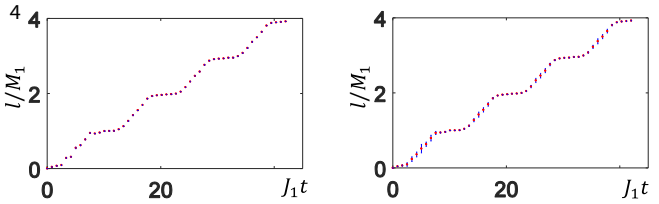

FIG. 9. (a) Center-of-mass displacements (red dots) and their standard deviations (blue error bars), which are calculated by assuming Gaussian distributed random on-site energy shift $\delta\omega_l = |l|\delta\omega$ due to deviations from the degeneracy. Standard deviations $\sigma(\delta\omega) = 0.05J_1$ and tunneling step $M_1 = 1$ corresponds to the zeroth stage of the multistage switch. $\delta\omega = 0.05J_1$ corresponds to $\sqrt{(X-F)(Y-F)} \simeq 10\ \mu$m. (b) The same as in (a) except that the tunneling step $M_1 = 10$, corresponding to the first stage of the multistage switch.

with $\delta\omega_l \simeq |l|\delta\omega$ and $\delta\omega \simeq 3\frac{\arccos(\frac{A+D}{2})}{2\pi}\Omega_F$ (unimportant global shift is ignored). Thanks to the topological protection, we find that our scheme works very well as long as the energy shift is smaller than the smallest band gap $\frac{|l|\delta\omega}{4J_1} \lesssim 1$, as confirmed by our numerical simulation shown in Fig. 9. Without loss of generality, we consider the above rectangular-shaped cavity with $F = 10$ cm. $\frac{\delta\omega}{4J_1}$ as a function of X and Y is shown in Fig. 6, and $\frac{|l|\delta\omega}{4J_1} \lesssim 1$ leads to $|l|\sqrt{(X-F)(Y-F)} \lesssim 1000$ μm. If we encode the quantum information in the space $l \in [-l_{\max}, l_{\max}]$ (i.e., the maximal OAM to be switched to is $|l| = l_{\max}$), our scheme works well when $l_{\max} \lesssim \frac{1000\mu\text{m}}{\sqrt{(X-F)(Y-F)}}$. Using standard micrometric linear translation stages, one can easily achieve an accuracy with $(X-F) \sim (Y-F) \sim \mu$m, thus corresponding $l_{\max}$ can be up to hundreds. A nanometer-precision linear translation stage (e.g., M-714.2HD, PI, Germany) can reach an accuracy of 0.05 μm, which yields a maximal usable OAM of several thousands in principle.

[1] M. A. Nielsen and I. L. Chuang, *Quantum Computation and Quantum Information* (Cambridge University, Cambridge, England, 2000).

[2] N. Gisin, G. Ribordy, W. Tittel, and H. Zbinden, Quantum cryptography, Rev. Mod. Phys. **74**, 145 (2002).

[3] D. Culcer, A. L. Saraiva, B. Koiller, X. Hu, and S. Das Sarma, Valley-Based Noise-Resistant Quantum Computation Using Si Quantum Dots, Phys. Rev. Lett. **108**, 126804 (2012).

[4] U. L. Andersen, J. S. Neergaard-Nielsen, P. Van Loock, and A. Furusawa, Hybrid discrete- and continuous-variable quantum information, Nat. Phys. **11**, 713 (2015).

[5] L. Allen, M. W. Beijersbergen, R. J. C. Spreeuw, and J. P. Woerdman, Orbital angular momentum of light and the transformation of Laguerre-Gaussian laser modes, Phys. Rev. A **45**, 8185 (1992).

[6] G. Molina-Terriza, J. P. Torres, and L. Torner, Twisted photons, Nat. Phys. **3**, 305 (2007).

[7] A. M. Yao and M. J. Padgett, Orbital angular momentum: Origins, behavior and applications, Adv. Opt. Photon. **3**, 161 (2011).

[8] M. Malik, M. Erhard, M. Huber, M. Krenn, R. Fickler, and A. Zeilinger, Multi-photon entanglement in high dimensions, Nat. Photon. **10**, 248 (2016).

[9] J. T. Barreiro, T.-C. Wei, and P. G. Kwiat, Beating the channel capacity limit for linear photonic superdense coding, Nat. Phys. **4**, 282 (2008).

[10] J. Wang *et al.*, Terabit free-space data transmission employing orbital angular momentum multiplexing, Nat. Photon. **6**, 488 (2012).

[11] F. Cardano *et al.*, Quantum walks and wavepacket dynamics on a lattice with twisted photons, Sci. Adv. **1**, e1500087 (2015).

[12] F. Cardano, M. Maffei, F. Massa, B. Piccirillo, C. de Lisio, G. De Filippis, V. Cataudella, E. Santamato, and L. Marrucci, Statistical moments of quantum-walk dynamics reveal topological quantum transitions, Nat. Commun. **7**, 11439 (2016).

[13] X.-W. Luo, X. Zhou, C.-F. Li, J.-S. Xu, G.-C. Guo, and Z.-W. Zhou, Quantum simulation of 2D topological physics in a 1D array of optical cavities, Nat. Commun. **6**, 7704 (2015).

[14] X.-F. Zhou, X.-W. Luo, S. Wang, G.-C. Guo, X. Zhou, H. Pu, and Z.-W. Zhou, Dynamically Manipulating Topological Physics and Edge Modes in a Single Degenerate Optical Cavity, Phys. Rev. Lett. **118**, 083603 (2017).

[15] X.-W. Luo, X. Zhou, C.-F. Li, J.-S. Xu, G.-C. Guo, C. Zhang, and Z.-W. Zhou, Synthetic-lattice enabled all-optical devices based on orbital angular momentum of light, Nat. Commun. **8**, 16097 (2017).

[16] R. Fickler, R. Lapkiewicz, W. N. Plick, M. Krenn, C. Schaeff, S. Ramelow, and A. Zeilinger, Quantum entanglement of high angular momenta, Science **338**, 640 (2012).

[17] R. Fickler, R. Lapkiewicz, M. Huber, M. P. J. Lavery, M. J. Padgett, and A. Zeilinger, Interface between path and orbital angular momentum entanglement for high-dimensional photonic quantum information, Nat. Commun. **5**, 4502 (2014).

[18] X.-L. Wang, X.-D. Cai, Z.-E. Su, M.-C. Chen, D. Wu, L. Li, N.-L. Liu, C.-Y. Lu, and J.-W. Pan, Quantum teleportation of multiple degrees of freedom of a single photon, Nature (London) **518**, 516 (2015).

[19] S. Gröblacher, T. Jennewein, A. Vaziri, G. Weihs, and A. Zeilinger, Experimental quantum cryptography with qutrits, New J. Phys. **8**, 75 (2006).

[20] M. Mafu, A. Dudley, S. Goyal, D. Giovannini, M. McLaren, M. J. Padgett, T. Konrad, F. Petruccione, N. Lutkenhaus, and A. Forbes, Higher-dimensional orbital-angular-momentum-based quantum key distribution with mutually unbiased bases, Phys. Rev. A **88**, 032305 (2013).

[21] G. Vallone, V. D'Ambrosio, A. Sponselli, S. Slussarenko, L. Marrucci, F. Sciarrino, and P. Villoresi, Free-Space Quantum key Distribution by Rotation-Invariant Twisted Photons, Phys. Rev. Lett. **113**, 060503 (2014).

[22] M. Mirhosseini, O. Magaña-Loaiza, M. O'Sullivan, B. Rodenburg, M. Malik, M. Lavery, M. Padgett, D. Gauthier, and R. Boyd, High-dimensional quantum cryptography with twisted light, New J. Phys. **17**, 033033 (2015).

[23] G. Thalhammer, R. W. Bowman, G. D. Love, M. J. Padgett, and M. Ritsch-Marte, Speeding up liquid crystal slms using overdrive with phase change reduction, Opt. Exp. **21**, 1779 (2013).

[24] M. Mirhosseini, O. S. Magana-Loaiza, C. Chen, B. Rodenburg, M. Malik, and R. W. Boyd, Rapid generation of light beams carrying orbital angular momentum, Opt. Exp. **21**, 30196 (2013).

[25] N. Radwell, D. Brickus, T. W. Clark, and S. Franke-Arnold, High speed switching between arbitrary spatial light profiles, Opt. Exp. **22**, 12845 (2014).

[26] M. J. Strain *et al.*, Fast electrical switching of orbital angular momentum modes using ultra-compact integrated vortex emitters, Nat. Commun. **5**, 4856 (2014).

[27] L. Marrucci, C. Manzo, and D. Paparo, Optical Spin-to-Orbital Angular Momentum Conversion in Inhomogeneous Anisotropic Media, Phys. Rev. Lett. **96**, 163905 (2006).

[28] S. Slussarenko, E. Karimi, B. Piccirillo, L. Marrucci, and E. Santamato, Efficient generation and control of different-order orbital angular momentum states for communication links, J. Opt. Soc. Am. A **28**, 61 (2011).

[29] F. D. M. Haldane and S. Raghu, Possible Realization of Directional Optical Waveguides in Photonic Crystals with Broken Time-Reversal Symmetry, Phys. Rev. Lett. **100**, 013904 (2008).
[30] M. Hafezi, E. A. Demler, M. D. Lukin, and J. M. Taylor, Robust optical delay lines with topological protection, Nat. Phys. **7**, 907 (2011).
[31] K. Fang, Z. Yu, and S. Fan, Realizing effective magnetic field for photons by controlling the phase of dynamic modulation, Nat. Photon. **6**, 782 (2012).
[32] Q. Lin and S. Fan, Light Guiding by Effective Gauge Field for Photons, Phys. Rev. X **4**, 031031 (2014).
[33] L. Lu, J. D. Joannopoulos, and M. Soljačić, Topological photonics, Nat. Photon. **8**, 821 (2014).
[34] L. Yuan, Y. Shi, and S. Fan, Photonic gauge potential in a system with a synthetic frequency dimension, Opt. Lett. **41**, 741 (2016).
[35] Q. Lin, M. Xiao, L. Yuan, and S. Fan, Photonic Weyl point in a two-dimensional resonator lattice with a synthetic frequency dimension, Nat. Commun. **7**, 13731 (2016).
[36] D. J. Thouless, Quantization of particle transport, Phys. Rev. B **27**, 6083 (1983).
[37] M. Lohse, C. Schweizer, O. Zilberberg, M. Aidelsburger, and I. Bloch, A Thouless quantum pump with ultracold bosonic atoms in an optical superlattice, Nat. Phys. **12**, 350 (2016).
[38] S. Nakajima, T. Tomita, S. Taie, T. Ichinose, H. Ozawa, L. Wang, M. Troyer, and Y. Takahashi, Topological thouless pumping of ultracold fermions, Nat. Phys. **12**, 296 (2016).
[39] Y. E. Kraus, Y. Lahini, Z. Ringel, M. Verbin, and O. Zilberberg, Topological States and Adiabatic Pumping in Quasicrystals, Phys. Rev. Lett. **109**, 106402 (2012).
[40] M. Verbin, O. Zilberberg, Y. Lahini, Y. E. Kraus, and Y. Silberberg, Topological pumping over a photonic fibonacci quasicrystal, Phys. Rev. B **91**, 064201 (2015).
[41] A. Celi, P. Massignan, J. Ruseckas, N. Goldman, I. B. Spielman, G. Juzeliunas, and M. Lewenstein, Synthetic Gauge Fields in Synthetic Dimensions, Phys. Rev. Lett. **112**, 043001 (2014).
[42] M. Mancini *et al.*, Observation of chiral edge states with neutral fermions in synthetic hall ribbons, Science **349**, 1510 (2015).
[43] B. K. Stuhl, H.-I. Lu, L. M. Aycock, D. Genkina, and I. B. Spielman, Visualizing edge states with an atomic bose gas in the quantum Hall regime, Science **349**, 1514 (2015).
[44] J. A. Arnaud, Degenerate optical cavities, Appl. Opt. **8**, 189 (1969).
[45] P. Horak, H. Ritsch, T. Fischer, P. Maunz, T. Puppe, P. W. H. Pinkse, and G. Rempe, Optical Kaleidoscope Using a Single Atom, Phys. Rev. Lett. **88**, 043601 (2002).
[46] S. Gopalakrishnan, B. L. Lev, and P. M. Goldbart, Emergent crystallinity and frustration with Bose-Einstein condensates in multimode cavities, Nat. Phys. **5**, 845 (2009).
[47] K. E. Ballantine, B. L. Lev, and J. Keeling, Meissner-like Effect for a Synthetic Gauge Field in Multimode Cavity QED, Phys. Rev. Lett. **118**, 045302 (2017).
[48] N. Schine, A. Ryou, A. Gromov, A. Sommer, and J. Simon, Synthetic Landau levels for photons, Nature (London) **534**, 671 (2016).
[49] A. Yariv and P. Yeh, *Photonics: Optical Electronics in Modern Communications* (Oxford University, Oxford, 2007).
[50] N. Hodgson and H. Weber, *Laser Resonators and Beam Propagation: Fundamentals, Advanced Concepts, Applications* (Springer, New York, 2005).
[51] S. S. R. Oemrawsingh, X. Ma, D. Voigt, A. Aiello, E. R. Eliel, G. W. t'Hooft, and J. P. Woerdman, Experimental Demonstration of Fractional Orbital Angular Momentum Entanglement of Two Photons, Phys. Rev. Lett. **95**, 240501 (2005).
[52] E. Karimi, B. Piccirillo, E. Nagali, L. Marrucci, and E. Santamato, Efficient generation and sorting of orbital angular momentum eigenmodes of light by thermally tuned q-plates, Appl. Phys. Lett. **94**, 231124 (2009).
[53] J. Leach, M. J. Padgett, S. M. Barnett, S. Franke-Arnold, and J. Courtial, Measuring the Orbital Angular Momentum of a Single Photon, Phys. Rev. Lett. **88**, 257901 (2002).
[54] S. Ganeshan and S. Das Sarma, Constructing a Weyl semimetal by stacking one-dimensional topological phases, Phys. Rev. B **91**, 125438 (2015).
[55] M. J. Rice and E. J. Mele, Elementary Excitations of a Linearly Conjugated Diatomic Polymer, Phys. Rev. Lett. **49**, 1455 (1982).
[56] D. F. Walls and G. J. Milburn, *Quantum Optics* (Springer-Verlag, Berlin, 2008).
[57] G. Hernández, *Fabry-Perot Interferometers* (Cambridge University, Cambridge, England, 1986).
[58] X. Bao, Y. Qian, J. Yang, H. Zhang, Z. Chen, T. Yang, and J.-W. Pan, Generation of Narrow-Band Polarization-Entangled Photon Pairs for Atomic Quantum Memories, Phys. Rev. Lett. **101**, 190501 (2008).
[59] B. Nagorny, Th. Elsässer, and A. Hemmerich, Collective Atomic Motion in An Optical Lattice Formed Inside a High Finesse Cavity, Phys. Rev. Lett. **91**, 153003 (2003).
[60] L. Marrucci, E. Karimi, S. Slussarenko, B. Piccirillo, E. Santamato, E. Nagali, and F. Sciarrino, Spin-to-orbital conversion of the angular momentum of light and its classical and quantum applications, J. Opt. **13**, 064001 (2011).
[61] H. K. Raut, V. A. Ganesh, A. S. Nair, and S. Ramakrishna, Anti-reflective coatings: A critical, in-depth review, Energy Environ. Sci. **4**, 3779 (2011).